Research Square

Preprints are preliminary reports that have not undergone peer review.
They should not be considered conclusive, used to inform clinical practice,
or referenced by the media as validated information.

Optimization and life-cycle assessment of biochar production through microwave–assisted pyrolysis of industrial hemp hurd

Nived S Menon
Indian Institute of Technology Bhubaneswar
Venkat Srinadh Rejeti
Indian Institute of Technology Bhubaneswar
Remya Neelancherry
remya@iitbbs.ac.in

Indian Institute of Technology Bhubaneswar

Research Article

Keywords: Hemp hurds, Microwave-assisted pyrolysis, Negative emission technology, Fuel replacement, Biochar optimization, Life-cycle assessment

Posted Date: February 20th, 2026

DOI: https://doi.org/10.21203/rs.3.rs-8918479/v1

License: This work is licensed under a Creative Commons Attribution 4.0 International License.
Read Full License

Additional Declarations: No competing interests reported.

Abstract

Industrial hemp hurds (HH) are the biomass residues following bast separation from inner core of hemp plant for fibre extraction. Current research emphasized on microwave-assisted pyrolysis (MAP) of HH for the optimization of hemp biochar (HB) production, its characterization and cradle to gate life cycle analysis (LCA) to explore its application as fossil fuels alternate. Utilizing central composite design (CCD), MAP was optimized for two operational parameters: microwave power (P) and pyrolysis time (T) with HB yield and higher heating value (HHV) as output parameters. The highest HB yield of 75.3% was obtained at P and T of 600 W and 10 min respectively with model Eq. 325.1 -0.37P -12.17T + 0.004PT + $1.3\times10\text{-}4P^2$ +$0.18T^2$, validated with an average error of 4.8%. The maximum HHV of 29.5 MJ/kg prevailed at 1000 W and 25 min with model Eq. 71.91 -0.18P -0.11T + $1.3\times10\text{-}4P^2$ and an average error of 5.2%. The negative greenhouse gas (GHG) emission of -10.06 t CO_2 e/yr suggested the sustainability of MAP for HB production through carbon capture. The life cycle assessment (LCA) using ReCiPe Midpoint (H) indicated that the HB production process significantly impacts several environmental categories, with the highest impact being on global warming potential, at 167.3 kg CO_2 eq. It is followed by human non-carcinogenic toxicity, at 3199.9 kg 1, 4-DCB, and terrestrial ecotoxicity, at 2380.1 kg 1, 4-DCB. The sensitivity analysis evaluated the environmental impacts derived from four distinct impact assessment methodologies, facilitating the identification of overarching trends in environmental impacts.

Novelty statement

The current study employed microwave-assisted pyrolysis (MAP) technique for biochar production from industrial hemp hurds. Biochar production was optimized using response surface methodology for maximizing heating value and yield emphasizing its applicability as a potential and sustainable fuel alternative. Detailed characterization studies like scanning electron microscopy, X-ray diffraction, Fourier transform infrared spectroscopy, Energy-dispersive X-ray spectroscopy, BET surface area analysis, etc., were performed to examine the quality of the obtained biochar. Apart from biochar production through advanced technology like MAP, this study also focused on the environmental impact of such process through a thorough investigation on negative emission technology potential and life-cycle assessment using cradle-to-gate approach. This research highlighted the negative greenhouse gas (GHG) emission of -10.06 t CO_2 e/yr suggesting the sustainability of MAP for biochar production through carbon capture.

Therefore, this research presents novel contributions to the field of waste valorization and renewable and clean energy production through biofuel production from MAP of waste biomass.

Highlights

• Industrial hemp hurd biochar (HB) prepared using microwave-assisted pyrolysis (MAP)

• 1000 W and 7 min residence time were optimum conditions for 37.6% HB yield

• Negative GHG emission of -10.1 t CO e/yr was determined for HB production

• 24.9 MJ/kg heating value and ~ 90% fixed carbon suggested better fuel applicability

• LCA of HB production assessed global warming potential with 167.3 kg CO eq.

1. Introduction

Waste biomass has plentiful reserves and is considered as a carbon-neutral feedstock, capable of substituting conventional fuels. Biomass can also be converted into various products using the pyrolysis process, which is a succession of endothermic (heating and dehydration) and exothermic (volatile emission) reactions which degrade biomass by heating in a dearth of oxygen [1]. Contemporary requirements demand energy-efficient pyrolysis techniques that produce better yields and superior biofuels. [2]. Microwave-assisted pyrolysis (MAP) is an excellent thermochemical technique to obtain biochar, bio-oil, and syngas, owing to its advantages over conventional processes, which include uniform heat distribution, minimized hazardous chemicals in bio-oil, simplicity of control, and expense minimization. [3], [4]. Current technique has been employed efficiently on various feedstock like agricultural residue [5], algae [6], sewage sludge [7], and different feedstocks [8], [9] to generate biofuels.

Biochar is an important product that is produced through biomass pyrolysis attenuating multi-faceted applications like fuel replacement, soil enhancer, carbon storage and as precursor for the synthesis of functional carbon-based compounds through subsequent modifications such as activation [10]. The chemical and energy characteristics of the biochar plays a pivotal role in determining their applicability for various purposes. The fixed carbon content and heating value are considered to be essential for energy application of biochar [11]. Similarly the biochar with greater surface area and porosity were considered for soil conditioning [12], and novel carbon-based compounds development. Such properties of biochar are significantly influenced by the feedstock characteristics and MAP operating conditions. MW power and time are observed to be the most influential parameters by many researches for converting variety of feedstock into biochar and biofuels [13]. Therefore, it is necessary to analyse the effect of these operating parameters in optimizing the production of biochar in required quantity and quality. Response surface methodology (RSM) technique is often used by the scientific community to statistically evaluate the effect of input parameters on the desired output. Moreover, the capability of CCD to study individual and combined effect of multi-factor input components with minimal experimental runs on the output reduces the time, cost and energy requirements. The experimental input data are subjected to an ANOVA analysis, which yields output data that is further processed to create the necessary mathematical models for determination of functional correlation between input and output variables [14].

Cannabis sativa L., known as industrial hemp, is being cultivated since decades for its fibre, oil, medical properties, and bioenergy potential. Industrial hemp, which is sometimes mistaken with Cannabis sativa L., does not contain enough THC to be intoxicated. Typically, it has 75% woody core (shives or hurds), 20% fibre, and 5% dust. Hemp hurd (HH) is the woody core of the stalk having long and short fibres. Such HH can be used to make fabric, paper/pulp, acoustic barriers, hybrid material boards etc. [15]. Under the

influence of climate change, this crop may serve as an effective means for carbon sequestration, attributed to its swift biomass production and substantial carbon sink ability [16]. Given the presence of lignocellulosic content in HH [17], bioenergy related synthesis [18] and biochar production through conventional pyrolysis [19] were researched recently. The drawbacks from biochar production through conventional pyrolysis like longer retention time, greater energy input requirement, etc. can be riposted through MAP technology for HH conversion, which is seldom explored.

CO_2 emissions constitute a major portion of global greenhouse gas emissions, and accounts for three-quarters of the overall greenhouse gas (GHG) emissions. A significant and immediate reduction in GHG emissions as well as adjustments in resource management are required in order to meet the climate targets that were established by the Paris Agreement. There are a variety of technology development and consumption shift that could be considered as potential pathways that could accomplish these aims [20]. Within the realm of technology-based solutions, there is a collection of scenarios that takes into consideration the widespread implementation of negative emissions technologies (NETs). Despite the fact that recent assessments have brought to light a dearth of bottom-up and upscaling research, which are essential for the actual development of the sector, discussions over the requirement, viability, and prevalence of NETs in the upcoming technological advances remains evolving [21]. Biochar is essential among various NETs, including afforestation and soil carbon sequestration, for apprehending atmospheric CO_2 and significantly contributes to achieving NetZero emission targets. Biochar is acknowledged for its capacity to sequester carbon, thereby aiding in climate change mitigation as a result of its high density of recalcitrant carbon. A key approach for evaluating the capacity of biochar to mitigate CO_2 emissions is through carbon crediting. This method functions as a regulatory mechanism for managing global GHG emissions in the context of the Kyoto Protocol. This scheme requires precise documentation of GHG storage and emissions [21]. The overall reduction of emissions is contingent upon GHG storage, whereas emissions from carbonisation significantly influence the diversity of total emissions. GHG emissions resulting from biochar production show considerable variability, which is affected by factors like feedstock characteristics, temperature, heating rate, and thermal conversion method employed. Woolf et al. predicted the NET potential of 0.27–0.49 Gt CO_2 e/year due to biochar production in terms of indirect air capture [22]. Similarly, Santos et al. forecasted that biochar production has the potential to mitigate emissions ranging from 1.0 to 1.8 Gt CO_2 annually across different circumstances [23]. A knowledge gap exists in systematically clarifying the influence of various factors on the diversity of CO_2 emissions in biochar production systems, especially at the life cycle stage.

Life cycle assessment (LCA) facilitates the identification of hotspots within a system and encourages the exploration of technological innovations that minimise energy consumption and environmental impact [24]. LCA framework consists of several processes, such as defining goals and scope, conducting inventory analysis, assessing life cycle impacts, and interpreting results where goal and scope definitions are instrumental in the explanation of the product system, which encompasses system boundaries and functional units [25]. Typically, the stages of product development are considered while defining system boundaries such as cradle-to-grave, cradle-to-gate, gate-to-gate, or gate-to-grave

boundary might be used, depending on the chosen scope. In contrast to the cradle-to-gate method, which typically disregards the usage and end-of-life phases, the cradle-to-grave approach takes into account the full product or process life cycle. However gate-to-gate solely considers production that takes place on the premises [26]. Many researches worked on LCA of biochar production from different waste feedstocks like forest residues [27], manure [28], agro-residues [29], woody biomass [30] etc. for different applications like soil systems [29], bioasphalt [31], bioenergy, and so on from a circular economy perspective [32]. However, no studies have been identified regarding the life cycle assessment of the MAP of HH.

The present work emphasized on the optimization of operating parameters for the production of biochar, using RSM for maximizing yield and higher heating value (HHV) from MAP of industrial hemp hurds (HH). Further, the potential environmental impacts of such system throughout its life cycle alongside the NET potential were analysed from a cradle-to-gate approach of life cycle assessment.

2. Materials and Methods

2.1. Materials and chemicals:

The HH obtained from a farm in Pauri, Uttarakhand, India, and harvested between June and August was air-dried, grinded to size less than 4.75 mm. Silicon carbide (SiC) was used as the microwave susceptor, procured from Vaishnavi Industrial Needs Pvt Ltd., India. Analytical FT-IR grade KBr (99% pure) was procured from Merck, India.

2.2. Microwave pyrolysis reactor:

This study employed a custom-designed microwave (MW) reactor, operated at a frequency of 2.45 GHz with a power control ranging from 200 W to 1000 W (Fig S1). A cylindrical quartz vessel with a diameter of 12 cm and a height of 20 cm was used as the reactor where 3 g of HH along with SiC balls as microwave susceptors was used per batch. N_2 gas was initially purged with a flow rate of 0.6 L/min for 10 min to create an oxygen-free environment and later reduced to 0.2 L/min during the MAP process. The obtained HH biochar (HB) was collected and corresponding yield was calculated using the Eq. 1.

$$HB\,yield\ (Y\,\%) = \frac{Weight\,of\,HB\ \ (g)}{Weight\,of\,HH\ \ (g)} \times\ 100$$

1

2.3. Response surface methodology (RSM):

RSM is one of the reliable tool for analysing the impact of different parameters on reactions. Central composite design (CCD) was employed in RSM to investigate the relationship between independent and dependent variables for the MAP experiments, as it a cost-effective approach to optimize variables and responses with minimum runs. The energy input to the system and the pyrolysis duration are two most

important process parameters of MAP. MW power (P) in the range of 500–1000 W and pyrolysis time (T) in the range of 10–28 min were considered based on the numerous previous trials on the MAP of HH. The Stat-Ease 360 Software (Version 22.0.4) was used to design the experimental runs, and the centre point was repeated five times to assess the repeatability of experiments. CCD generated experimental runs with factorial points (2^k), axial points (2 k), and replicated center points (n_k), where 'k' represents the number of independent parameters. The number of experiments to be conducted (N) was determined using Eq. 2.

$$N = 2^k + 2k + n_k = 2^2 + 2\,(2) + 5 = 13$$

2

The HB yield (Y %) and higher heating value (HHV) were chosen as the responses of the experimental runs. These variables were analysed using ANOVA, 3D graph and contour plot. Further, statistical analysis was conducted, including the F-value (Fisher variation ratio), *p*-value (probability), regression coefficient (R^2), and adequate precision (AP), to determine the relevance, importance, and suitability of the model used.

2.4. HB characterization:

The specific surface area of HB was determined based on the N_2 adsorption-desorption method using a BET surface area analyzer (QUADRASORB SI, Quantachrome Instruments, USA). The microscopic structure was studied using scanning electron microscopy (SEM, MERLIN compact, Carl Zeiss, Germany) equipped with energy-dispersive X-ray spectroscopy (EDS, 51XMX 1004, Oxford Instruments, UK) to provide detailed information on surface elemental composition. X-ray diffraction analysis (XRD, D8 Advance, Bruker, Germany) and Fourier transform infrared spectroscopy (FTIR, Alpha-FTIR, Bruker, Germany) were used to identify the various surface-functional elements and crystalline structure, respectively. Proximate analysis, the moisture content (MC), volatile matter (VM), ash content (AC), and fixed carbon content (FC), were measured as per standard methods [33]. The elemental composition (C, H, and O) in weight percentage was determined by using Nhuchhen's formula to the proximate analysis data as stated in Eq. 3–5 [34]. Higher heating value (HHV) was determined using a bomb calorimeter (RSB-5, Rajdhani Co. Lim, New Delhi, India).

$$C = -35.9972 + 0.7698 \times\ VM + 1.3269 \times\ FC + 0.3250 \times\ AC$$

3

$$H = 55.3678 - 0.4830 \times\ VM - 0.5319 \times\ FC - 0.5600 \times\ AC$$

4

$$O = 223.6805 - 1.7226 \times\ VM - 2.2296 \times\ FC - 2.2463 \times\ AC$$

5

2.5. Emission estimation from HB Production

2.5.1 Emission factor estimation

The estimation of emission factor (EF) are done considering the most likely combinations of biochar production factors such carbonization process, scale, excess energy usage, and feedstock type. Kavindi, Tang, and Sasaki 2025 reported various estimated EFs considering different potential biochar production factors by classifying in to 24 groups considering 1 ton of biochar production as standard functional unit. MAP of HH is a carbonization technique for producing HB along with varied quantities of bio-oil and syngas. Both the volatiles can be additionally bolstered for energy applications in terms of electricity generation or satisfying thermal energy requirement for feedstock pre-drying. Therefore, MAP is considered to be closed carbonization technique with surplus energy utilization facility. The current study falls under the class 17, where the carbonization scale tends to be unspecified for closed carbonization system with surplus energy utilization ability [35].

2.5.2 Scenario-specific GHG emission estimation

Considering unpopular HH cultivation in India, the average annual HH production (M_{HH}) is assumed to be 100 t/yr along with the utilization rate of the crop residue (u) of 100% (since HH alone is considered as feedstock) as per [35]. The specific scenario of HB production (M_{HB}) was determined using Eq. 6.

$$M_{HB} = M_{HH} \times Y_{HB} \times u \times m$$

6

Where, Y_{HB} denotes the HB yield on dry weight of HH basis, and m refers to the MC of HH. The scenario specific GHG reduction (t CO_2 e/yr) is calculated as represented in Eq. 7.

$$Total\ GHG\ emission = E - S$$

7

Where, *E* and S refers to the annual GHG emissions (t CO_2 e/yr) occurred and the annual GHG storage (t CO_2 e/yr) by HB respectively in a particular scenario. E and S were determined using the subsequent Eq. 8–9.

$$E = M_{HB} \times EF$$

8

$$S = M_{HB} \times C_{org} \times C_{st} \times \frac{44}{12}$$

9

Where, C_{org}, C_{st} refer to organic carbon content of HB (assumed mean value- 0.57), and stable carbon content fraction of HB after 100 years (0.8). The coefficient 44/12 represents the carbon dioxide fraction. The negative value of total GHG emission represents the positive effect of the HB production on environment through carbon sequestration. Conversely, the positive value of total GHG emission denotes the negative impact of HB production on environment.

2.6. Life Cycle Analysis (LCA) methodology:

2.6.1. Goal and scope

Cradle-to-gate life cycle analysis (LCA) with 1 ton of HH as functional unit was performed to evaluate the environmental impacts of HB production from HH using MAP to identify the hotspots and potential environmental trade-offs associated and provide recommendations for improvement [25]. The scope of this LCA includes the following processes as depicted in Fig. 1.

The environmental impact categories assessed were global warming potential, acidification potential, eutrophication potential, ozone depletion potential and photochemical oxidant potential. The data were derived from research articles and databases such as Ecoinvent (Version 3.9), the Indian Life Cycle Inventory Database and Agribalyse database [36]. The geographical scope of the study was limited to the production of HB from HH in India. Further, the study assumed average conditions for the production process and variations in regional conditions or management practices were not considered.

All energy required for the process was obtained from the electricity grid and a uniform composition and energy content of HH was assumed throughout the year. Due to practical and theoretical constraints, certain features like the impacts of equipment manufacturing, MW susceptor production, construction activities and materials used for infrastructure development, the participation of human resources, and the overhead generated by lighting and maintenance of the facilities were excluded from the study, either because they did not affect the results or were standardized.

2.6.2. Impact assessment methodology

The environmental impacts of HB production were assessed using the openLCA 1.11.0 software, a professional tool for modelling and analysing the life cycle of products, processes, and services transparently while following ISO 14040 recommendations. Four different impact assessment methodologies were used to provide a comprehensive understanding of the environmental impacts of MAP. The EDIP method was used to evaluate the environmental impacts of HB production across its entire life cycle, from resource extraction to disposal, considering a broad range of environmental impacts such as climate change, acidification, and eutrophication. The CML 2001 method, on the other hand, focused on the potential for HB production to cause damage to human health and ecosystems through the release of pollutants assessing impacts such as ozone depletion, photochemical oxidant formation, and toxic emissions to air, water, and soil [37]. The ReCiPe Midpoint (H) and ILCD 2.0 2018 methods aimed to provide a comprehensive assessment of environmental impacts of HB across a range of impact categories including global warming, ozone depletion, photochemical oxidation, acidification,

eutrophication, terrestrial ecotoxicity, human toxicity and water depletion [38], [39]. The impact assessment method was limited to quantitative modelling of early stages in the cause-effect chain to reduce uncertainties. Sensitivity analysis of the LCA was carried out using the LCA inventory and assessing them using above-mentioned impact assessment methodologies. The analysis considers four impact categories: global warming potential, ozone depletion, photochemical oxidation, and acidification.

2.6.3. Life cycle inventory (LCI)

The cultivation of hemp plants, its transportation from farm to factory, decortication, size reduction, MAP for HB production and pelletization were the unit processes considered as different phases of HB production. Certain assumptions were considered in this study as follows. Around 2 kg of hemp seeds were considered as input and nitrogen, phosphorus, and potassium-rich fertilizers were added in amounts of 2.5 kg, 1.25 kg, and 1.75 kg, respectively for plant growth [40]. A sprinkler system was assumed for irrigating the land of 0.525 m^2 area with 40 cm of water depth for a growing season, obtaining 1350 kg of hemp plant, which is transported to factory (15 km) using 2-axle trailer with carrying capacity of 3 t. Micro-Decorticator (MD100, HurdMaster) with a capacity to operate at 50 kg/h, having a power rating of 1.5 kW, was considered for decortication, i.e., to separate the fibre from the hurds. After decortication, 1000 kg of HH were obtained with size < 4.75 mm. A screw conveyor (LS250, Henan Green Eco-equipment) was considered to feed the dried ground feedstock into the pyrolysis reactor with the screw diameter, pitch, and rotational speed were 250 mm, 250 mm, and 50 rpm, respectively, delivering feedstock at a rate of 0.3327 m^3/h and consuming 1.327 kW power, and has a capacity of 4000 kg/h. The MW reactor (Twin Engineers, Haryana) was operated at the optimized parameters of 1000 W MW power for 7 min. The operating parameters were decided based on the results obtained in this study. A pellet-making machine manufactured by Vinspire Agrotech was used for pelletization which operated at a power of 3728.5 W (5hp) and yielded an output of 100 kg/hr.

3. Results and Discussion

3.1. Central composite design

The results from 13 experimental runs were displayed in Table 1. HB yield and HHV ranged from 9.7% to 75.3% and 12.5 MJ/kg to 29.5 MJ/kg respectively. The lowest HB yield (9.7%) and highest HHV (29.5 MJ/kg) was obtained at 1000 W and 25 min with an energy consumption of 0.42 kWh. While the highest HB yield (75.3%) and lowest HHV (12.5 MJ/kg) was obtained at 600 W and 10 min with an energy consumption of 0.10 kWh.

Table 1
HB yield, and HHV obtained at different process parameters of MAP of HH

Run	P (W)	T (min)	Y (%)	HHV (MJ/kg)	Energy consumed (kWh)
1	800 (0)[a]	17.5 (0)	20.3	15.7	0.23
2	500 (-α)	17.5 (0)	55.8	14.1	0.15
3	800 (0)	17.5 (0)	20.7	14.4	0.23
4	800 (0)	28 (+α)	16.6	15.5	0.37
5	600 (-1)	25 (+ 1)	29.7	13.7	0.25
6	600 (-1)	10 (-1)	75.3	12.5	0.10
7	1000 (+α)	10 (-1)	28.7	25.4	0.16
8	1000 (+α)	17.5 (0)	10.4	28.8	0.29
9	800 (0)	7 (-α)	64.4	12.6	0.09
10	800 (0)	17.5 (0)	20.5	14.2	0.23
11	1000 (+α)	25 (+ 1)	9.7	29.5	0.42
12	800 (0)	17.5 (0)	20.4	14.5	0.23
13	800 (0)	17.5 (0)	19.2	14.6	0.23

[a] : Coded level in parentheses

3.1.1. Effect of process parameters on HB yield

The highest HB yield of 75.3% was obtained at a MW power of 600 W and a residence time of 10 min. Such operating conditions resulted in minimal thermal degradation of the feedstock, allowing most of the volatile matter (VM) to remain in the HB. In contrast, the least HB yield (9.7%) was observed at 1000 W and 25 min operating conditions. The progressive elongation of the reaction time results in a reduction in HB yield attributing to the secondary processes, namely gasification, volatilization and thermal cracking. Moreover, an intermediate combination of these factors resulted in moderate HB yield. The interactive effect of MW power and residence time is depicted by the 3-D surface plot (Fig. 2 (a)) highlighting the importance of controlling these process parameters to optimize HB production. It can be inferred that the variation in MW power at lower residence time (5–15 min) reduced the HB yield drastically, as supported by the literature [41]. Whereas at higher residence time (15–28 min), little variation in HB yield was observed across different MW powers (500 W – 1000 W). It can be attributed to possible promotion of the breakage of long carbon chains at higher residence times resulting in higher volatile content liberation leading to reduced HB yield.

3.1.2. Effect of process parameters on HHV

The 3-D surface plot of HHV is shown in Fig. 2 (b). The highest heating value (HHV) of 29.5 MJ/kg was obtained at a MW power of 1000 W and pyrolysis time of 25 min. MW power input of 1000 W and residence time of 25 min resulted in nearly complete pyrolysis of the feedstock, producing HB with greater HHV. Higher MW power (1000 W) and moderate residence time (25 min) enabled more extensive polymers to crack into smaller aromatic rings and carbon-carbon bonds, increasing HHV. A nearly complete breakdown of feedstock rendered HB richer in carbonaceous content with higher heating value. In contrast, the least HHV (12.5 MJ/kg) was observed at 600 W and 10 min operating conditions. MW power of 800 W applied for a shorter duration (7 min) resulted in insufficient feedstock cracking, producing HB with lower heating value (12.6 MJ/kg) due to lower carbon content. The interaction between MW power (800–1000 W) and residence time (7–25 min) significantly influenced the HHV of HB. At 1000 W, increasing residence time from 10 to 25 min increased the HHV from 25.4 MJ/kg to 29.5 MJ/kg, highlighting the dominance of residence time. On the other hand, at residence time of 17.5 min, increasing power from 800 W to 1000 W raised the HHV from 14.2 MJ/kg to 28.8 MJ/kg, demonstrating the more significant impact of a higher MW power. An intermediate combination of factors (1000 W and 17.5 min) yielded HB with an HHV of 28.8 MJ/kg.

3.1.3. Model development and corresponding statistical analysis

The experimental results were fitted to four regression models: linear model, 2-factor interaction model (2FI), quadratic and cubic model using design expert software, represented in Table S1. The models were analysed based on their sequential p-value, lack of fit p-value, and adjusted and predicted R^2 value. Based on the model statistics for HB yield, the quadratic model is suggested as it has a significantly lower p-value of < 0.0001 depicted in Table 3. Furthermore, the model F-value of 1396.4 implies that the model is significant implying only a 0.01% chance that an F-value this large could occur due to noise. The model tends to be more reliable with the observed standard deviation (SD) and mean value of 0.9 and 30.1, implying consistent predictions with less variability, offering acceptable baseline for individual forecasts. The coefficient of variation (CV) of 2.9%, represents the normalized measure of the dispersion of the dataset. Predicted R^2 was 0.994, while adjusted R^2 was 0.998, with variation less than 0.2, suggesting a high correlation. The P, T, PT, P^2 and T^2 were the significant model terms with p-values < 0.0001. The lack of fit was also non-significant with p-value of 0.1140 (> 0.05), which is desirable for the model to fit. Adequate Precision measures the signal-to-noise ratio of 110.8 > 4 indicated an adequate signal. The reported equation according to the quadratic model by considering significant terms is mentioned as Eq. 10.

$$Y\ (\%) = 325.10 - 0.37P - 12.17T + 0.004PT + 1.30 \times\ 10^{-4}P^2 + 0.18 \times\ T^2$$

10

Based on the model statistics for HHV, the quadratic model is suggested as it has significantly lower p-value of < 0.0001. The F-value of the model is 110.9, and its p-value is < 0.0001, indicating that the model is significant. It can be observed from the Table 2 that the F-value of MW power stands at 218.1 and 189.7 for individual (P) and quadratic term (P^2) respectively, with p-value < 0.0001 in both the cases. The lack of fit F-value of 4.1 implies that the lack of fit is insignificant with p-value of 0.1 (> 0.05) relative to the pure error. There is a 10.3% chance that a lack of fit F-value this large could occur due to noise. The adjusted R^2 for the model is 0.971, while the predicted R^2 for the model is 0.924, indicating a better correlation. Adequate Precision measures the signal-to-noise ratio of 29.3 (> 4) indicates an adequate signal. The reported equation according to the quadratic model by considering significant terms is reported as Eq. 11.

$$HHV\ (MJ/kg) = 71.91 - 0.18P - 0.11T + 1.30 \times\ 10^{-4}P^2$$

11

Table 2
ANOVA of developed model for HB yield and HHV and model terms

Terms	**HB yield**		**HHV**	
	***F*-value**	***p*-value**	***F*-value**	***p*-value**
Model	1396.4	< 0.0001	110.9	< 0.0001
P-MW power	2534.2	< 0.0001	218.1	< 0.0001
T-Reaction time	1579.6	< 0.0001	6.4	0.0398
PT	230.7	< 0.0001	2.6	0.1509
P^2	189.7	< 0.0001	189.7	< 0.0001
T^2	944.1	< 0.0001	0.33	0.5845
Lack of Fit	3.8	0.1140	4.1	0.1031
SD	0.9		0.9	
Mean	30.1		17.3	
C.V. %	2.9		5.2	
R^2	0.999		0.980	
Adjusted R^2	0.998		0.971	
Predicted R^2	0.994		0.924	
Adequate Precision	110.8		29.3	

3.1.4. Model Validation

The HB yield and HHV model was validated through three sets of experiments. In the first experiment, the dependent parameters were taken to be maximum and the independent values to be within the experimental range. The software offered one hundred solutions under the described circumstances from which single solution was chosen. Since the MW power input to the reactor could only be in multiples of one hundred, the solution was predicated on the highest desire and MW power being a multiple of one hundred. Additionally, two sets of runs within the range were undertaken at random. The experimental and anticipated values for each of the three runs are shown in Table S2. The average error of 4.8%, and maximum error of 5.5% was observed between the experimental and predicted HB yield. The maximum error of 6.6% and average error of 5.2% was observed in case of HHV, suggesting the adequacy of the model with minimal errors.

3.1.5. Result optimization

Process optimization was carried out to find the optimum value of independent parameters for the maximum HHV of resulting HB by targeting the HB yield to be 42.5%. This was done using the response surface models and the desirability function. The objective of maximizing HB yield and HHV guided the determination of ideal factor levels. The yield and HHV ranges considered for optimization were those achieved across the experimental runs, i.e., 9.7–75.3% and 12.5–29.5 MJ/kg, respectively. Table S3 shows the optimized solutions where the factor combination of 1000 W power and 30 mins residence time has the lowest desirability of 0.31. The factor combination of 1000 W power and 7 mins residence time provided the highest desirability of 0.52 and could be the optimized condition. Such operating conditions predicted the HB yield of 37.6% and maximum HHV of 24.9 MJ/kg. The obtained HB was analysed for further characterization.

3.2. Characterization of HH and HB:

3.2.1. Chemical characteristics

The chemical characteristics of the HH and HB are listed in Table 3, which includes proximate, ultimate analysis, and HHV.

Table 3
Chemical properties of HH and HB

Parameter (wt %)	HH	HB
MC	9.85 ± 0.19	1.21 ± 0.57
VM	79.20 ± 1.46	5.19 ± 1.63
AC	17.00 ± 0.08	3.61 ± 1.52
FC	4.80 ± 0.068	89.96 ± 0.22
C	37.86	88.55
H	5.20	2.97
O	34.68	6.01
H/C	1.65	0.40
O/C	0.69	0.05
HHV (MJ/kg)	11.08	24.9

The HH characteristics were within the range mentioned in the literature [42]. The MC of HB was 1.21%, enabling proper storage conditions. Conversion of HH to HB lowered VM and AC by 93.4%, and 78.7% respectively with 18.7 times increase in FC due to significant release of volatiles during MAP. The H/C and O/C ratios of HB were determined to be 0.40 and 0.05 respectively, suggesting its higher aromaticity and thermal stability [25]. Furthermore, the HHV of HB (24.9 MJ/kg) increased by 124.73% compared to the corresponding HH, suggesting its applicability as a fuel replacement, as the HHV of Indian coals lie in the range of 20–26 MJ/kg [43].

3.2.2. Thermogravimetric analysis

The thermogravimetric analysis (TGA) and derivative thermogravimetry (DTG) curves for HH biomass showed 10% weight loss at an initial stage from 30 ℃ up to approximately 300°C (Fig. 3), due to moisture loss and volatilization of low molecular weight components. A more rapid weight loss of around 50–60% occurred from 300°C to 400°C, with maximum rate of weight loss at 370 ± 10°C (0.5%/°C). This stage likely corresponds to the thermal decomposition of hemicellulose, cellulose, and lignin components of HH. The broad, asymmetrical shape of DTG peak suggested the HH decomposition occurred via multiple overlapping reactions. Beyond 400°C, a shoulder and slower continued weight loss was observed, indicating the residual decomposition of char and ash forming components up to 500°C. The total weight loss over the analysed temperature range was 80–85%, leaving inorganic char residue of 10–12% by weight. No exothermic decomposition reactions were detected based on the DTG curve, suggesting the HH decomposes via endothermic reactions in a relatively controlled, and non-explosive manner.

3.2.3. Physical characteristics of HB

The SEM image (Fig. 4 (a)) showed that the HB fibres appear primarily cylindrical, with an average diameter of 20–30 μm and length of 100–200 μm. It was observed to be moderately porous, with small pores (5–10 μm) visible between fibre bundles and along the length of fibres, possibly due to gas exchange and insulation ability. The fibre surfaces also showed fine transverse grooves and pits, which increases the surface area. These surface characterisitcs could regulate aspects like adsorption, dyeability or other surface-related attributes [44]. From the EDS data as observed in Fig. 4 (b), the main elemental composition of HB appeared to be carbon (82.6 wt. %), oxygen (16.8 wt. %) and calcium (0.5 wt. %), with C and O peaks dominating the spectra, similar to ultimate analysis results, as mentioned in Table 3.

Figure 4 (c) depicted a linear segment at low pressures, a plateau at high pressures, and an inflexion point in between, indicating the occurrence of mesopores in the material. BET study determined a specific surface area of 19.15 m^2/g which implies significant surface availability for adsorption, and potentially useful for pollutant separation, catalysis [45], and monitoring technologies [44]. The obtained surface area is within the range mentioned in the literature (18.23–25.38 m^2/g) for HH biochar produced through conventional pyrolysis [46].

The XRD diffractogram (Fig. 4 (d)) displayed prominent peak at θ = 7.6° (d-spacing = 5.82 Å) associated with the (1 0 1) lattice plane reflection of cellulose I, which is crystallised in a triclinic unit cell according to JCPDS number 50–2241. Minor impurity phases of quartz and calcite are also detected based on additional peaks at 2θ = 10.9°, 12.6°, 20.9° and 30.0° which may index to the (1 1 0) plane of aluminium, (0 0 4) plane of calcite, (0 2 0) plane of quartz and composite of quartz (JCPDS number 46–1045) and calcite (JCPDS number 5–586) respectively. The average crystallite size of 6.09 nm, calculated using the Scherrer equation for the (1 0 1) cellulose I peak, assuming a shape factor of 0.9 and Cu Kα wavelength of 0.15406 nm which indicated the presence of relatively small cellulose I crystallites in the material.

The FTIR spectrum (Fig. 4 (e)) of HB exhibited an intense broad absorption band in the 3000–3500 cm^{-1} region, indicating O–H stretching vibrations attributable to hydroxyl functional groups. The sharp peak in the 3500–3750 cm^{-1} region could indicate the presence of –OH stretching [47]. Multiple peaks between 2750 cm^{-1} and 3250 cm^{-1} signify asymmetric and symmetric C–H stretching modes of aliphatic alkanes. Prominent peaks between 1500 cm^{-1} and 1750 cm^{-1} depicts C = C double bond stretching vibrations of alkenes. The position and intensity of the absorption bands suggested that HB contains a mixture of alcohols, aldehydes or carboxylic acids, alkenes, and esters related surface functional groups. A strong absorption band at 1729 cm^{-1} corresponds to the carbonyl C = O stretching vibration, indicating the presence of aldehydes, ketones, carboxylic acids, or esters. Minor peaks observed between 1400 cm^{-1} and 1500 cm^{-1} are assignable to N–H bending vibrations of amines and C–H in-plane bending modes. A small peak at 1200 cm^{-1} can be attributed to the C–O stretching of ethers or esters [48].

Overall, the FTIR spectrum provided evidence for the presence of hydroxyl, alkane, alkene, carbonyl, amino and ether functional groups on the HB surface.

3.3. Estimation of negative emission during HB production

MAP of HH is a carbonization technique for producing HB along with varied quantities of bio-oil and syngas. Both the volatiles can be additionally bolstered for energy applications in terms of electricity generation or satisfying thermal energy requirement for feedstock pre-drying. Therefore, MAP is considered as closed carbonization technique with surplus energy utilization facility. EF was estimated for HB production using MAP based on two scenarios, namely (i) without surplus energy utilization and (ii) with surplus energy utilization. The surplus energy utilization refers to the additional energy sources from the byproducts obtained from MAP of HH (biooil and syngas). The EF in both the cases were determined to be 0.10 t CO_2 e/t HB (EF group 6), and − 0.78 t CO_2 e/t HB (EF group 17), derived from unspecified carbonization scale of wood residues suggested in the works of [35], detailed in Table S4. HB yield on dry weight of HH basis was calculated as cir. 41.7%. As per Eq. 6 the specific scenario annual HB production of 4.11 t/yr was estimated, considering 100 t of HH production annually, leading to the annual GHG storage of 6.86 t CO_2 e/yr. However, the GHG emissions of 0.41 t CO_2 e/yr, and − 3.20 t CO_2 e/yr were determined in case of without surplus and with surplus energy utilization scenarios respectively. Overall, the total GHG emissions of -6.45 t CO_2 e/yr, and − 10.06 t CO_2 e/yr were estimated in both the scenarios. The negative GHG emission implies the sustainable applicability of the MAP for conversion of HH into HB.

3.4. Life cycle impact assessment

Table S5 comprehensively overviews the environmental impact of producing HB based on the ReCiPe Midpoint (H) impact assessment method. The results indicated that the HB production significantly impacts several environmental categories, with the highest impact being on global warming potential, at 167.35 kg CO_2 eq., followed by human non-carcinogenic toxicity, at 3199.92 kg 1, 4-DCB, and terrestrial ecotoxicity at 2380.14 kg 1, 4-DCB. These results suggested that efforts to mitigate the environmental impact of the production process should focus on reducing greenhouse gas emissions and minimizing the application of chemicals that may negatively affect human health and ecosystems.

Table S6 provides information on the emissions associated with different stages of the HB production. It was observed that, hemp farming has a negative impact on global warming potential, with a value of -2.94 kg CO_2 eq., indicating that hemp plants absorb carbon dioxide during their growth, which helps mitigate the effects of greenhouse gas emissions. However, hemp farming has little impact on photochemical oxidant and acidification, with values of $1.11*10^{-3}$ kg ethylene eq. and $9.13*10^{-3}$ kg SO_2 eq., respectively with no impact on ozone depletion or eutrophication. The harvesting stage significantly impacts all environmental factors, with the highest impact on acidification, at 4.50 kg SO_2 eq., which is likely due to the use of heavy machinery and associated emissions. The transportation stage also significantly impacts global warming potential, with a value of 47.83 kg CO_2 eq., as well as a small

impact on photochemical oxidant and eutrophication. HB production through MAP has no impact on global warming potential or ozone depletion, but it does significantly impact photochemical oxidant, with a value of 1.99 kg ethylene eq., which may be linked to the emission of non-condensable gases during MAP. Other allied activities significantly impact all environmental factors, with the highest impact on photochemical oxidant, at $5.32*10^{-2}$ kg ethylene eq.

3.5. Sensitivity analysis:

The sensitivity analysis also shows that the choice of impact assessment method can affect the results of the LCA. Table S7 details the environmental impacts in the different stages of HB production and compares the results against the four impact assessment methodologies to gauge the robustness of the LCA. The results indicate that the impact of different stages of hemp farming varies significantly depending on the impact category being considered. For instance, the analysis shows that the global warming potential is primarily driven by harvesting, while the impact of ozone depletion is primarily driven by the allied activities.

3.5.1. Global Warming:

The GWP results of the different methods (depicted in Fig. 5 (a)) show relatively small variations for hemp farming, harvest, and transportation stages, indicating a consistent impact across all methods. All methods estimated a very small environmental impact for the electricity use stage, with values ranging from 0.08 to 0.1 kg CO_2 eq., since the electricity consumed in the process was assumed to be generated from renewable sources or have low carbon emissions. On the other hand, the HB production stage shows significant differences in the GWP impact estimates between the methods. The EDIP method estimates the highest impact with a value of 49.58 kg CO_2 eq., while the other methods, CML 2001, ReCiPe Midpoint (H), and ILCD 2.0 2018, estimate a value of 0 kg CO_2 eq. Due to incomplete combustion and volatile organic compound emissions, the EDIP method assumes that HB production releases many greenhouse gases, primarily CH_4 and N_2O. However, the other methods do not consider these emissions and assume that the HB production process is carbon-neutral or has a low carbon impact.

3.5.2. Ozone depletion:

The results (Fig. 5 (b)) for ozone depletion potential were generally low for all four impact assessment methods. The CML 2001 and ReCiPe Midpoint (H) methods gave identical results (~ $1.3*10^{-5}$ kg CFC-11 eq.), while ILCD 2.0 2018 method gave slightly higher results. Such variation can be attributed to differences in the underlying data and modelling assumptions used by each method. These results aligns with previous studies [17] showing that hemp cultivation has a low environmental impact compared to other crops due to its low requirements for fertilizers and pesticides.

3.5.3. Photochemical oxidation:

According to the results (Fig. 5 (c)), the photochemical oxidant impact from hemp farming, harvesting, allied and electricity production was relatively small across all methods. However, HB production and transportation had a higher impact in this category due to potential release of pollutants, such as volatile organic compounds and nitrogen oxides, react with sunlight and oxygen in the atmosphere to form photochemical smog. The CML 2001 method indicated that HB produced a photochemical oxidant impact of 2.84 kg ethylene-eq. Similarly, the ILCD 2.0 2018 method estimated a photochemical oxidant impact of 1.99 kg ethylene-eq. for HB production. The ReCiPe Midpoint (H) method also showed a higher impact on HB production than other processes, with a value of 1.99 kg ethylene-eq.

3.5.4. Acidification:

The results of the sensitivity analysis (Fig. 5 (d)) showed that the acidification potential of the HB production system varied depending on the impact assessment method used. The EDIP method had the lowest acidification potential, while the ILCD 2.0 2018 method had the highest in both harvesting (5.57 kg SO_2 eq.), transportation (0.48 kg SO_2 eq.) and allied stages (0.24 kg SO_2 eq.) of HB production. The differences in the acidification potential between the methods can be attributed to several factors, including differences in the characterization factors used to calculate the potential, the inclusion or exclusion of specific emissions, and the modelling assumptions used in each method. The ILCD 2.0 2018 method included an uncertainty factor to account for the potential impacts of acidification on freshwater and terrestrial ecosystems, which may result in a higher acidification potential than the other methods.

4. Conclusion

This study focused on the optimization of HB production from MAP of HH both in terms of yield and higher heating value (HHV). MW power of 1000 W and pyrolysis time of 7 min was found to be optimum solution yielding around 35% of HB with HHV of ~ 25 MJ/kg. The HHV of HB improved by around 125% compared to HH (11 MJ/kg). HB appeared moderately porous, with tiny pores (5–10 μm) evident between fibre bundles and along their length. Additionally, HB showcased higher fixed carbon (90%), lower moisture content (1.2%) and volatile matter (5.2%), suggesting its applicability as a sustainable fuel replacement in energy sector. The negative GHG emission of -10.06 t CO_2 e/yr suggested the sustainability of MAP for HB production through carbon capture. Further, this study assessed the environmental impact that the MAP treatment of HH has during its whole life cycle through the application of openLCA software (using ReCiPe midpoint method). The highest impact on global warming potential, at 167.35 kg CO_2 eq., followed by human non-carcinogenic toxicity, at 3199.92 kg 1, 4-DCB, and terrestrial ecotoxicity, at 2380.14 kg 1,4-DCB was observed, suggesting its impact on environment.

Abbreviations

AC

Ash content
AP
Adequate precision
CCD
Closed composite design
C_{org}
organic carbon content of HB
C_{st}
stable carbon content fraction of HB after 100 years
CV
Coefficient of variation
DCB
Dichlorobenzene
E
Annual GHG emissions occurred
EF
Emission factor
FC
Fixed carbon
FT-IR
Fourier transform infrared spectroscopy
GHG
Greenhouse gas
HB
Hemp hurd biochar
HH
Industrial hemp hurds
HHV
Higher heating value
LCA
Life-cycle Assessment
MAP
Microwave-assisted Pyrolysis
MC
Moisture content
MHB
Scenario specific annual average HB production
MHH
Annual average hemp hurd production
MW

Microwave
NET
Negative emission technology
RSM
Response surface methodology
S
Annual GHG storage
SD
Standard deviation
SEM
Scanning electron microscope
SiC
Silicon carbide
TGA
Thermogravimetric analysis
u
residue utilization rate
VM
Volatile matter
XRD
X-ray diffraction
YHB
HB yield in terms of dry weight of HH

Declarations

Authors Contribution

Nived S Menon: Investigation, Data analysis; Formal analysis; Writing-Original draft preparation; **Rejeti Venkat Srinadh**: Data curation, Methodology, Data analysis and validation, Writing-Original draft preparation; **Neelancherry Remya**: Supervision, Conceptualization, Funding acquisition, Writing-review and editing

Acknowledgements

This research was supported by Indian Institute of Technology Bhubaneswar, India

Funding

This research did not receive any specific grant from funding agencies in the public, commercial, or not-for-profit sectors.

Data Statement

All data used during the study appear in the presented article.

Declaration of Interests

Authors have nothing to declare.

References

1. Cisse I, Hernandez-Charpak YD, Diaz CA, Trabold TA (2022) Biochar Derived from Pyrolysis of Common Agricultural Waste Feedstocks and Co-pyrolysis with Low-Density Polyethylene Mulch Film. Waste Biomass Valoriz 13(9):3913–3932. 10.1007/s12649-022-01760-7
2. Usevičiūtė L, Baltrėnaitė-Gedienė E (2021) Dependence of pyrolysis temperature and lignocellulosic physical-chemical properties of biochar on its wettability. Biomass Convers Biorefinery 11:2775–2793. 10.1007/s13399-020-00711-3
3. Qiu T, Li C, Zhao W, Naz MY, Zhang Y (2024) Microwave-assisted pyrolysis of biomass: Influence of feedstock and pyrolysis parameters on porous biochar properties, *Biomass and Bioenergy*, vol. 193, no. October p. 107583, 2025. 10.1016/j.biombioe.2024.107583
4. Zhu H, Saddler J, Bi X (2022) An economic and environmental assessment of biofuel produced via microwave-assisted catalytic pyrolysis of forest residues. Energy Convers Manag 263:115723. 10.1016/j.enconman.2022.115723
5. Potnuri R, Venkata D, Sankar C, Yadav A, Sridevi V, Remya N (2023) A review on analysis of biochar produced from microwave-assisted pyrolysis of agricultural waste biomass, *J. Anal. Appl. Pyrolysis*, vol. 173, no. March, p. 106094, Aug. 10.1016/J.JAAP.2023.106094
6. Aggarwal M, Remya N (2021) Application of Native Mix Algal Strain for Gray Water Treatment and Biofuel Production: Preliminary Study. J Hazard Toxic Radioact Waste 25(2):04020070. 10.1061/(asce)hz.2153-5515.0000582
7. Kim D, Kim G, Oh DY, Seong KW, Park KY (2022) Enhanced hydrogen production from anaerobically digested sludge using microwave assisted pyrolysis. Fuel 314:123091. 10.1016/j.fuel.2021.123091
8. Zhang Z et al (2022) Microwave assisted catalytic pyrolysis of bagasse to produce hydrogen. Int J Hydrogen Energy 47(84):35626–35634. 10.1016/j.ijhydene.2022.08.162
9. De La Iturbides R, Jauregui Haza U, Polaert I (2022) Recent technological innovations on continuous microwave assisted biomass pyrolysis and perspectives for industrial scale applications. Bioresour Technol Rep 19:101202. 10.1016/j.biteb.2022.101202
10. Zhao R et al (Dec. 2021) Fabrication and environmental applications of metal-containing solid waste/biochar composites: A review. Sci Total Environ 799:149295. 10.1016/J.SCITOTENV.2021.149295

11. Liu Y, Yang X, Zhang J, Zhu Z (2022) Process Simulation of Preparing Biochar by Biomass Pyrolysis Via Aspen Plus and Its Economic Evaluation. Waste Biomass Valoriz 13(5):2609–2622. 10.1007/s12649-021-01671-z
12. Danesh P, Niaparast P, Ghorbannezhad P, Ali I (Apr. 2023) Biochar Production: Recent Developments, Applications, and challenges. Fuel 337:126889. 10.1016/J.FUEL.2022.126889
13. Mohit A, Remya N (2023) Optimization of biochar production from greywater grown polyculture microalgae using microwave pyrolysis. Bioresour Technol 388:129666. 10.1016/j.biortech.2023.129666
14. Tripathi M, Bhatnagar A, Mubarak NM, Sahu JN, Ganesan P (Oct. 2020) RSM optimization of microwave pyrolysis parameters to produce OPS char with high yield and large BET surface area. Fuel 277:118184. 10.1016/J.FUEL.2020.118184
15. Raja T, D Y (2023) Analysis of the properties of a hemp fibre derived from Cannabis sativa as a renewable source. Biomass Convers Biorefinery 13:15149–15159. 10.1007/s13399-023-04861-y
16. Biswakarma N, Kailashpati T, Arya S, Harshang T Industrial Hemp in India: A Booming Botanical Wonder with Endless Potentials, *Food and Scientific Reports*, vol. 4, no. 10, pp. 60–67, Oct. 2023. [Online]. Available: https://foodandscientificreports.com/details/industrial-hemp-in-india-a-booming-botanical-wonder-with-endless-potentials.html
17. Ahmed ATMF, Islam MZ, Mahmud MS, Sarker ME, Islam MR (Jan. 2022) Hemp as a potential raw material toward a sustainable world: A review. Heliyon 8(1):e08753. 10.1016/J.HELIYON.2022.E08753
18. Antorán D et al (2023) Waste Hemp Hurd as a Sustainable Precursor for Affordable and High-Rate Hard Carbon-Based Anodes in Sodium-Ion Batteries. Energy Fuels 37(13):9650–9661. 10.1021/acs.energyfuels.3c01040
19. Ravindra B, Malabadi KP, Kolkar RK, Chalannavar M, Acharya, Mudigoudra BS Industrial Cannabis sativa-Hemp: Biochar applications and disadvantages, *World J. Adv. Res. Rev.*, vol. 20, no. 1, pp. 371–383, 2023, [Online]. Available: https://wjarr.com/content/industrial-cannabis-sativa-hemp-biochar-applications-and-disadvantages
20. Azzi ES, Karltun E, Sundberg C (2019) Prospective life cycle assessment of large-scale biochar production and use for negative emissions in stockholm. Environ Sci Technol 53:8466–8476. 10.1021/acs.est.9b01615
21. Woolf D, Lehmann J, Ogle S, Kishimoto-Mo AW, McConkey B, Baldock J (2021) Greenhouse Gas Inventory Model for Biochar Additions to Soil. Environ Sci Technol 55(21):14795–14805. 10.1021/acs.est.1c02425
22. Woolf D, Amonette JE, Street-Perrott FA, Lehmann J, Joseph S (2010) Sustainable biochar to mitigate global climate change. Nat Commun 1(5). 10.1038/ncomms1053
23. Santos FM, Gonçalves AL, Pires JCM (2019) Negative emission technologies. Bioenergy Carbon Capture Storage Using Nat Resour Sustain Dev 1–13. 10.1016/B978-0-12-816229-3.00001-6

24. Li Y, Gupta R, Zhang Q, You S (2022) Review of biochar production via crop residue pyrolysis: Development and perspectives, *Bioresour. Technol.*, vol. 369, no. November p. 128423, 2023. 10.1016/j.biortech.2022.128423
25. Venkata Srinadh R, Neelancherry R (2023) Technoeconomic and sustainability analysis of agricultural waste conversion technologies, *Agric. Waste to Value-Added Prod.*, vol. 1, pp. 47–68, Nov. https://doi.org/10.1007/978-981-99-4472-9_3
26. Andooz A, Eqbalpour M, Kowsari E, Ramakrishna S, Ansari Cheshmeh Z (Feb. 2023) A comprehensive review on pyrolysis from the circular economy point of view and its environmental and social effects. J Clean Prod 388:136021. 10.1016/J.JCLEPRO.2023.136021
27. Puettmann M, Sahoo K, Wilson K, Oneil E (2020) Life cycle assessment of biochar produced from forest residues using portable systems. J Clean Prod 250:119564. 10.1016/j.jclepro.2019.119564
28. Fernandez-Lopez M, Puig-Gamero M, Lopez-Gonzalez D, Avalos-Ramirez A, Valverde J, Sanchez-Silva L (2015) Life cycle assessment of swine and dairy manure: Pyrolysis and combustion processes. Bioresour Technol 182:184–192. 10.1016/j.biortech.2015.01.140
29. Zhu X et al (2022) Life-cycle assessment of pyrolysis processes for sustainable production of biochar from agro-residues. Bioresour Technol 360:127601. 10.1016/j.biortech.2022.127601
30. Shaheen J, Fseha YH, Sizirici B (2022) Performance, life cycle assessment, and economic comparison between date palm waste biochar and activated carbon derived from woody biomass. Heliyon 8(12):e12388. 10.1016/j.heliyon.2022.e12388
31. Zhou X et al (2020) Life Cycle Assessment of Biochar Modified Bioasphalt Derived from Biomass. ACS Sustain Chem Eng 8(38):14568–14575. 10.1021/acssuschemeng.0c05355
32. Carvalho J et al (2022) Life Cycle Assessment (LCA) of Biochar Production from a Circular Economy Perspective. Processes 10. doi.org/10.3390/pr10122684
33. APHA (2013) Standard methods for the examination of water and wastewater, 23rd ed., American Water Works Association/American Public Works Association/Water Environment Federation. 10.2105/SMWW.2882
34. Nhuchhen DR (Sep. 2016) Prediction of carbon, hydrogen, and oxygen compositions of raw and torrefied biomass using proximate analysis. Fuel 180:348–356. 10.1016/J.FUEL.2016.04.058
35. gajasinghe AG, Kavindi L, Tang, Sasaki Y (2025) Assessing GHG Emission Reduction in Biomass-Derived Biochar Production via Slow Pyrolysis: A Cradle-to-gate LCA Approach. Resour Conserv Recycl 212:107900. https://doi.org/10.1016/j.resconrec.2024.107900
36. Petri E et al (2024) Conversion of biodigestate into activated carbon for electrochemical application: Process performance and life cycle assessment. Carbon N Y 226. https://doi.org/10.1016/j.carbon.2024.119221
37. San Juan JLG, Ching PML, Mayol AP, Culaba AB, Ubando A Envinronmental Life Cycle Analysis of Algal Biorefineries for Biofuel Production under the Circular Economy Concept, (2020) *IEEE 12th Int. Conf. Humanoid, Nanotechnology, Inf. Technol. Commun. Control. Environ. Manag. HNICEM 2020*, pp. 0–4, 2020. 10.1109/HNICEM51456.2020.9400011

38. Gievers F, Loewen A, Nelles M (2021) Life cycle assessment of sewage sludge pyrolysis: Environmental impacts of biochar as carbon sequestrator and nutrient recycler, *Detritus*, vol. 16, no. September, pp. 94–105. 10.31025/2611-4135/2021.15111
39. Papageorgiou A, Azzi ES, Enell A, Sundberg C (Jul. 2021) Biochar produced from wood waste for soil remediation in Sweden: Carbon sequestration and other environmental impacts. Sci Total Environ 776:145953. 10.1016/J.SCITOTENV.2021.145953
40. Pratap Singh Verma P, Kumar A, Prawal Pratap Singh Verma C, Padalia R, Singh V, Agri B (2019) Effect of nitrogen, phosphorus and potassium levels on growth and yield of turmeric (Curcuma longa L.) Under the Katyur valley of western Himalayan region of Uttarakhand. ~ 117 ~ J Med Plants Stud 7(2):117–122
41. Nazari M, Aguilar MM, Ghislain T, Lavoie JM (2024) Microwave-assisted pyrolysis of biomass waste for production of high-quality biochar: Corn stover and hemp stem case studies. Biomass Bioenergy 187:107302. 10.1016/j.biombioe.2024.107302
42. Mankeed P, Onsree T, Naqvi SR, Shimpalee S, Tippayawong N (Mar. 2022) Kinetic and thermodynamic analyses for pyrolysis of hemp hurds using discrete distributed activation energy model. Case Stud Therm Eng 31:101870. 10.1016/J.CSITE.2022.101870
43. Gholizadeh M, Meca S, Zhang S, Clarens F, Hu X (Jun. 2024) Understanding the dependence of biochar properties on different types of biomass. Waste Manag 182:142–163. 10.1016/J.WASMAN.2024.04.011
44. Srinadh RV, Remya N, Verma A (2024) Biochar as a Filter Media for Air Pollution Control Systems. In: Neelancherry R, Gao B, Wisniewski Jr A (eds) in Agricultural Waste to Value-Added Products. Springer Nature Singapore, Singapore, pp 105–123. doi: https://doi.org/10.1007/978-981-97-2535-9_5.
45. Selvam M S and, Paramasivan B (2022) Microwave assisted carbonization and activation of biochar for energy-environment nexus: A review. Chemosphere 286:131631. 10.1016/j.chemosphere.2021.131631
46. Angin D, Şensöz S (2014) Effect of Pyrolysis Temperature on Chemical and Surface Properties of Biochar of Rapeseed (Brassica napus L). Int J Phytorem 16:7–8. 10.1080/15226514.2013.856842
47. Rubangakene NO, Elwardany A, Fujii M, Sekiguchi H, Elkady M, Shokry H (2023) Biosorption of Congo Red dye from aqueous solutions using pristine biochar and ZnO biochar from green pea peels. Chem Eng Res Des 189:636–651. 10.1016/j.cherd.2022.12.003
48. Sim DHH, Tan IAW, Lim LLP, Lau ET, Hameed BH (Jan. 2024) Synthesis of tapioca starch/palm oil encapsulated urea-impregnated biochar derived from peppercorn waste as a sustainable controlled-release fertilizer. Waste Manag 173:51–61. 10.1016/J.WASMAN.2023.11.006

Figures

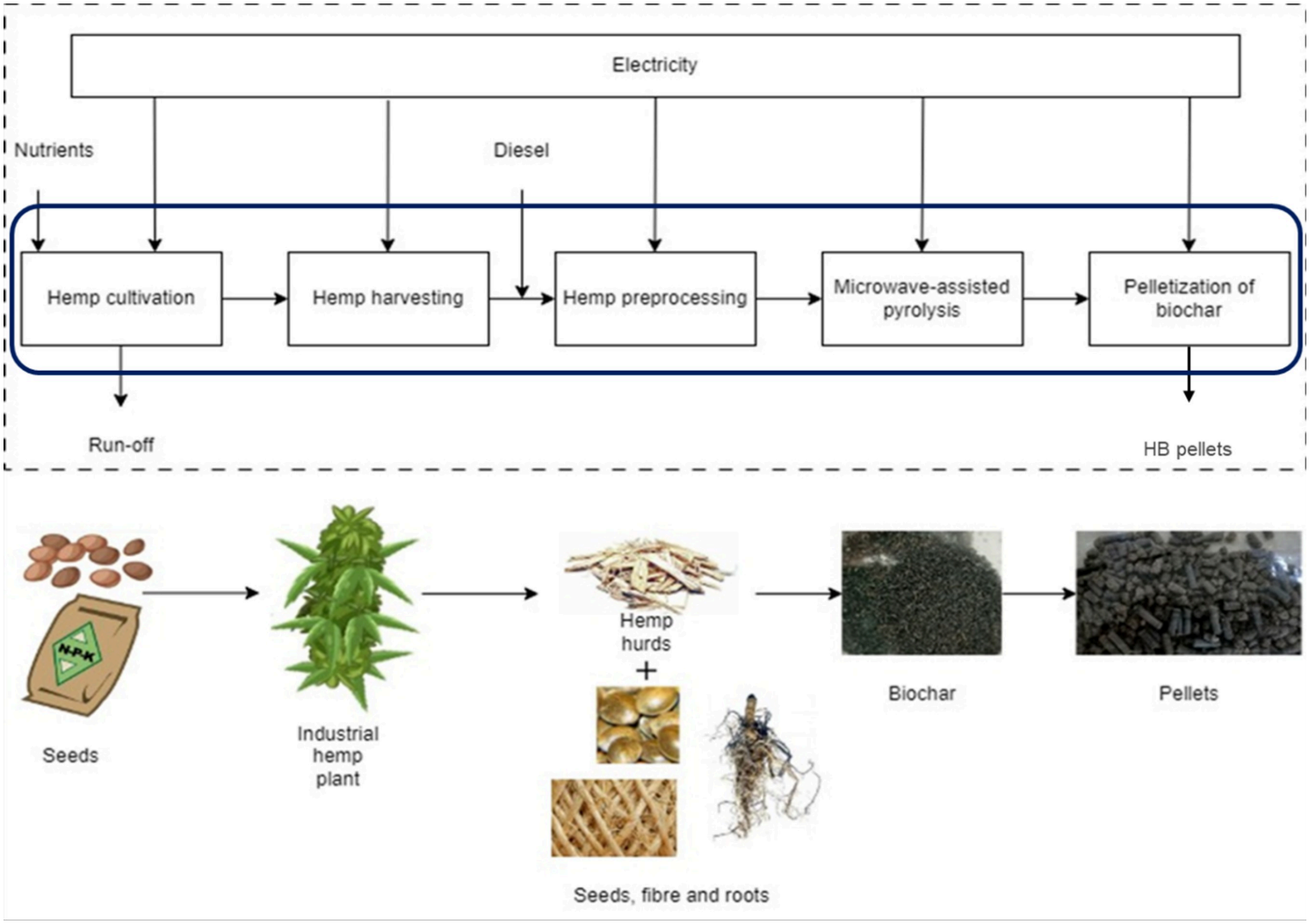

Figure 1

System boundary (inner box) and product flow for LCA of MAP of HH

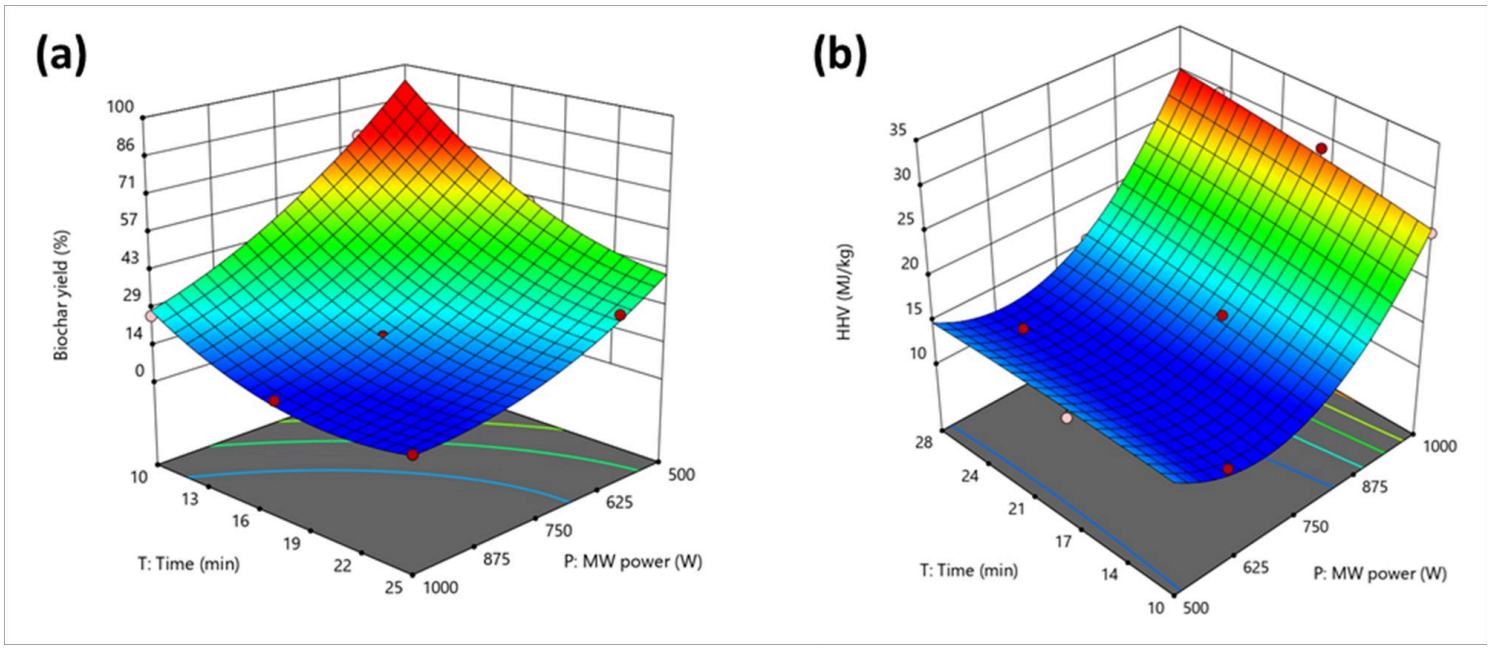

Figure 2

3-D response surface plots of (a) HB yield, and (b) HHV depicting the effect of MW power and reaction time

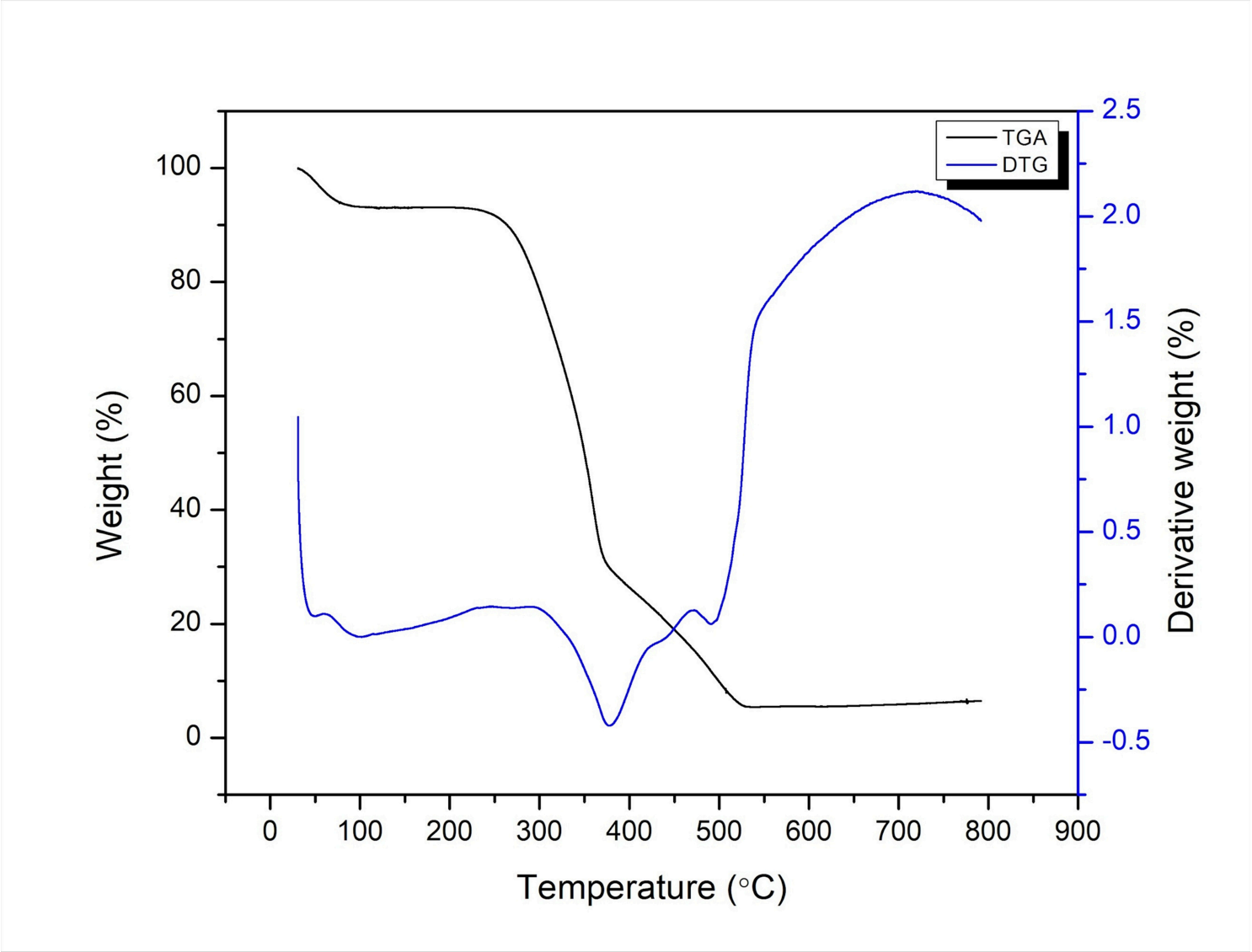

Figure 3

TGA and DTG curves of HH

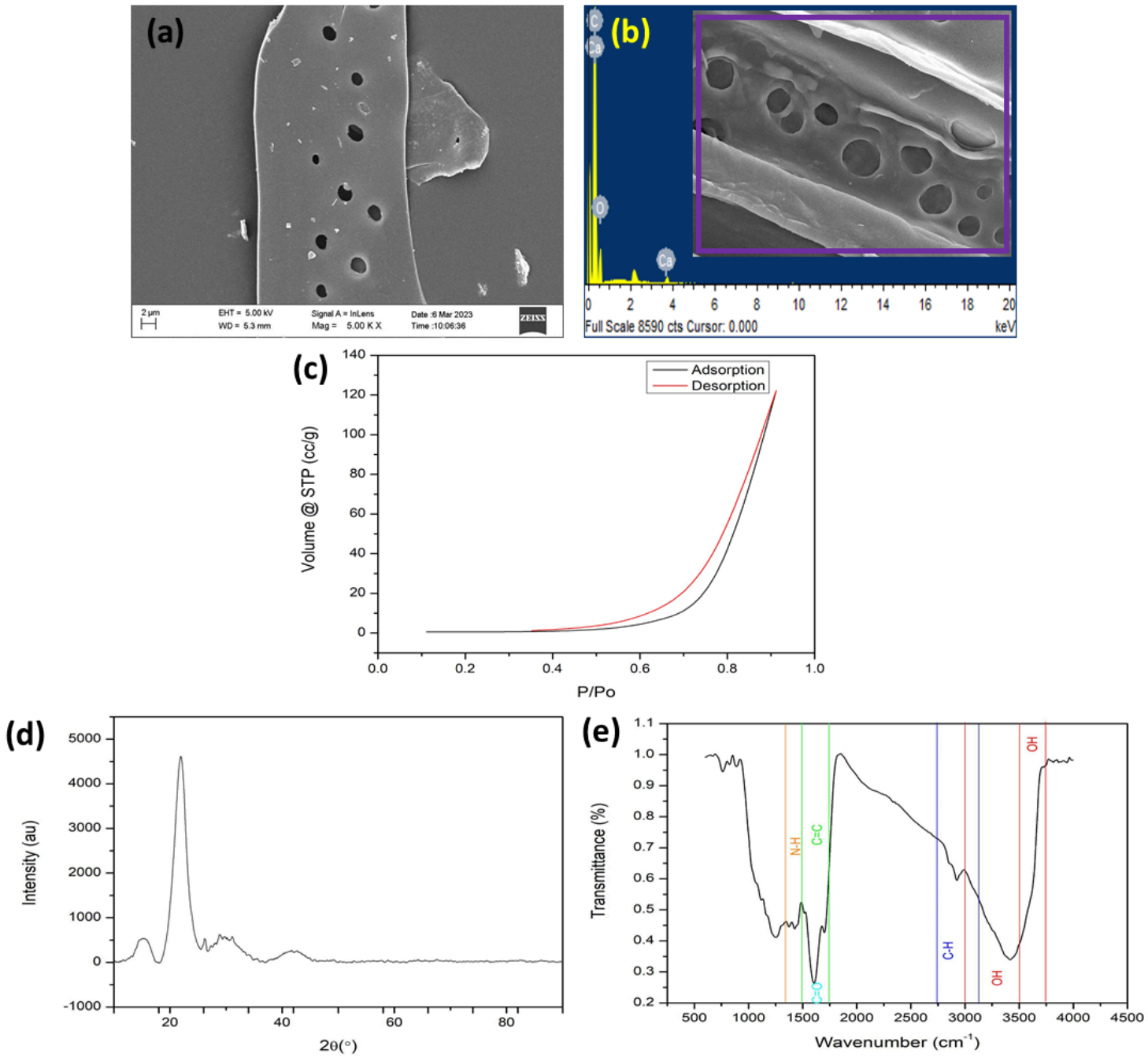

Figure 4

(a) SEM image, (b) EDS spectrum, (c) N_2 adsorption -desorption isotherm, (d) XRD pattern and (e) FT-IR spectrum of HB

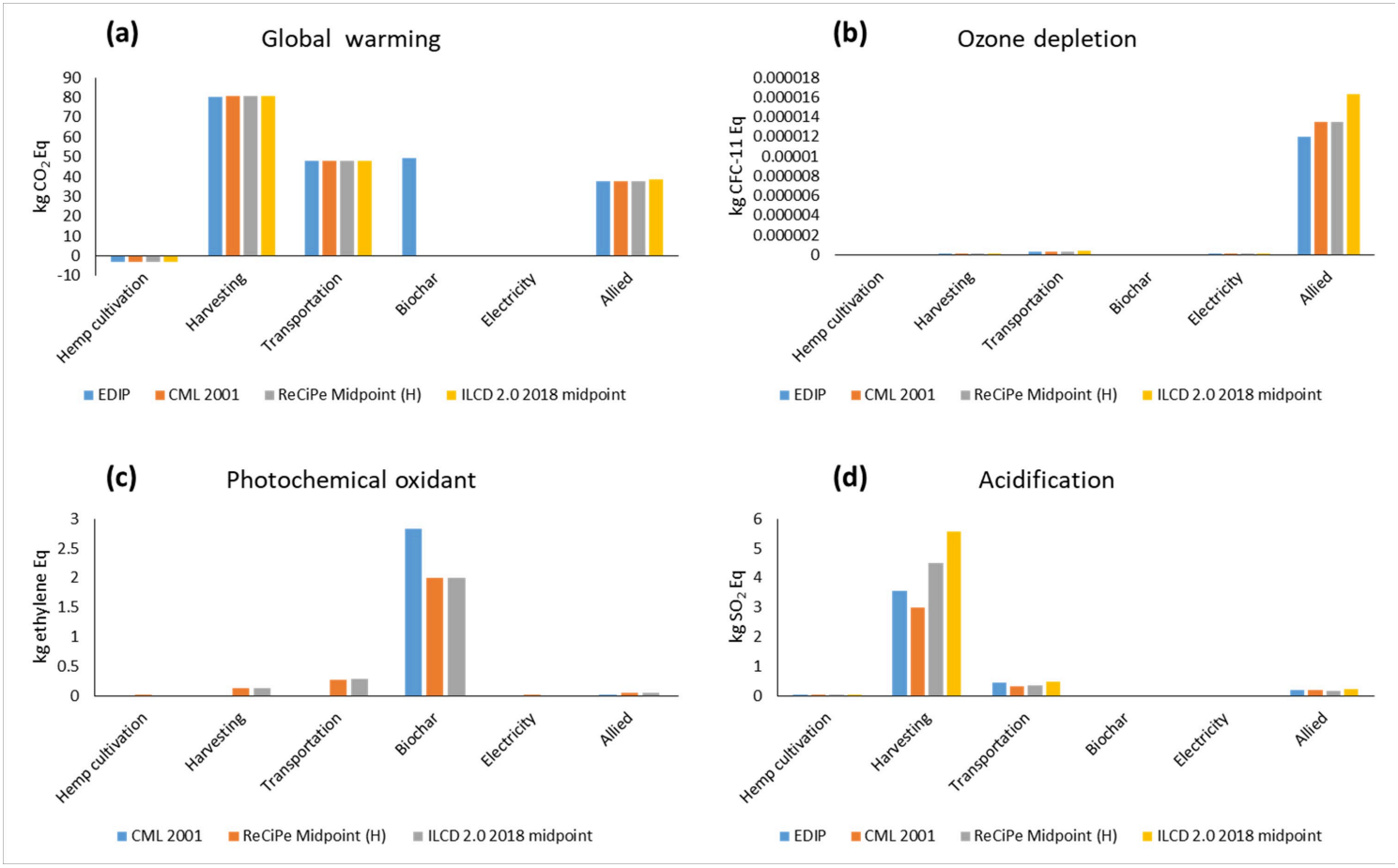

Figure 5

Environmental impacts in the different stages of HH biochar production

Supplementary Files

This is a list of supplementary files associated with this preprint. Click to download.

- Supplementarymaterial.docx